Performance Evaluation of the Herschel/SPIRE Instrument Flight Model Imaging Fourier Transform Spectrometer

Locke D. Spencer*[a], David A. Naylor[a], Baoshe Zhang[a], Peter Davis-Imhof[b], Trevor R. Fulton[b], Jean-Paul Baluteau[c], Marc J. Ferlet[d], Tanya L. Lim[d], Edward T. Polehampton[d], Bruce M. Swinyard[d]

[a]University of Lethbridge, 4401 University Drive, Lethbridge, Alberta, T1K 3M4, Canada, www.uleth.ca/phy/naylor/;

[b] Blue Sky Spectroscopy, Lethbridge, Alberta, T1J 0N9, Canada, www.blueskyinc.ca;

[c] Laboratoire d'Astrophysique de Marseille, 38 rue Frédéric Joliot-Curie, 13388 Marseille cedex 13, France, www.oamp.fr/lam/;

[d]Space Science and Technology Department, Rutherford Appleton Laboratory, Chilton, Didcot, Oxfordshire, OX11 0QX, UK, www.sstd.rl.ac.uk.

ABSTRACT

The Spectral and Photometric Imaging Receiver (SPIRE) is one of three scientific instruments onboard the European Space Agency (ESA)'s Herschel Space Observatory. The low to medium resolution spectroscopic capability of SPIRE is provided by an imaging Fourier transform spectrometer of the Mach-Zehnder configuration. Instrument performance of the SPIRE flight model was evaluated during a series of test campaigns. The SPIRE instrument performance verification was completed with instrument delivery to ESA in early 2007. In this paper we present the resulting performance characteristics of the SPIRE spectrometer flight model as determined from these test campaigns. We verify the instrument's conformance with fundamental design specifications such as spectral coverage and resolution. Variations across the imaging array of such properties as spectral resolution, vignetting, and instrumental line shape are explored. Additionally, instrumental artefacts observed during final verification testing are identified and quantified; with explanations provided for potential causes, and proposed methods to minimize their impact on scientific observations described.

Keywords: Herschel, SPIRE, Fourier transform spectrometer, spectral coverage, vignetting, instrumental line shape, imaging spectroscopy

1. INTRODUCTION

The Spectral and Photometric Imaging Receiver (SPIRE)[1] is one of three scientific instruments on ESA's Herschel Space Observatory.[2] Herschel features a 3.5 m diameter primary mirror which is passively cooled to ~80 K. SPIRE contains a two band imaging Fourier transform spectrometer (FTS) and a three band imaging photometer; providing the low to medium resolution spectroscopic capabilities of SPIRE over the $194 - 672$ μm wavelength region. A schematic diagram of the SPIRE spectrometer is shown in Figure 1. A calibration source (SCAL) at the second input port of SPIRE is used in order to compensate for the blackbody emission of the passively cooled telescope observed through the primary input port. Also shown in the figure are the two beamsplitters (BS1 & BS2), the SPIRE mirror mechanism (SMEC) which creates the optical path difference (OPD) between the two paths within the interferometer, and the two output ports which feed light to the complementary long and short wavelength detector arrays, SLW and SSW respectively.

The analysis presented in this work is based upon data obtained during flight model instrument verification tests, namely the first proto-flight model test (PFM1) through to the fifth and final PFM test, PFM5. The PFM tests were conducted between February 2005 and March 2007 at the Rutherford Appleton Laboratory (RAL) in the UK. We discuss the performance specifications of the SPIRE spectrometer[3] as driven by the science requirements of the Herschel key observing programs.[2]

*E-mail: Locke.Spencer@uLeth.ca, Telephone: 1 403 329 2719, Fax:1 403 329 2057

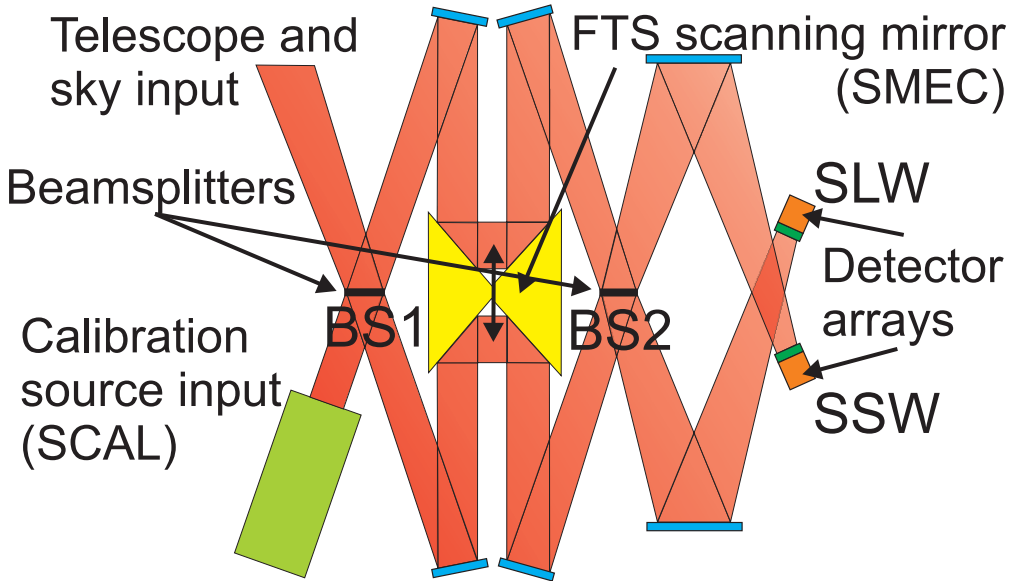

Figure 1. Schematic diagram of the SPIRE Fourier transform spectrometer.

2. INSTRUMENT PERFORMANCE

The fully integrated SPIRE imaging FTS was tested in a series of PFM test campaigns. Vibration testing was also performed on the SPIRE instrument to simulate the environmental conditions expected during the launch of Herschel.[4] A summary of the performance verification tests conducted during the PFM test campaigns, as related to the SPIRE imaging FTS, is given below:[5]

- Low, medium, and high resolution FTS scans with various infrared sources across the detector arrays (i.e. internal and external blackbodies, various molecular laser lines, photonic mixer lines, and the ambient room background).
- Medium resolution FTS scans for the investigation of input port balancing at various SCAL settings (see Section 2.2).
- Tests of various SPIRE Astronomical Observation Template (AOT) scripts.
- Tests to verify SMEC performance characteristics.

In the following subsections, the performance of the SPIRE FTS as it pertains to optical bandpass, instrument line shape, spectral resolution, obliquity effects, vignetting, straylight, input port compensation, fringe contrast, and mechanical performance is described. Summary tables are presented in Sections 2.2.2 & 2.3, conclusions, open issues, and recommendations are presented in Section 3.

2.1 Optical Performance

2.1.1 Spectrometer Bandpass

The edges of the SPIRE spectrometer wavebands (SLW and SSW) are defined as the points where the spectral intensity is one half of its average single-mode in-band value. In order to focus on the response of the detectors themselves, the contributions to the measured spectrum from the internal input sources, i.e. the cold blackbody (CBB) and SCAL, were removed.[6] The measured edges of the spectrometer wavebands shown in Table 1 are the average ($\pm 1\sigma$) for the active pixels in each array.

The waveband edges as measured during each of PFM3–PFM5 showed no significant differences. As such, the band edges for the SLW array, as well as the high-wavenumber (short-wavelength) SSW band edges meet

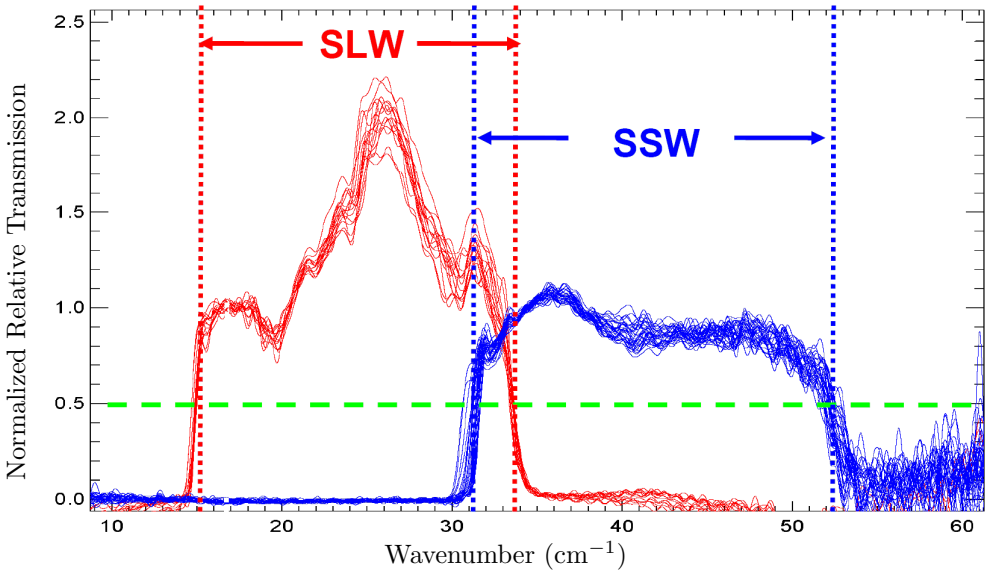

Figure 2. SPIRE spectrometer flight model SLW and SSW frequency bands.

Table 1. SPIRE Frequency Bands

Band	Edge	Specification (cm^{-1})	Measured (cm^{-1})
SLW	cut-on	$14.64 - 15.02$	14.91 ± 0.10
	cut-off	$33.00 - 33.67$	33.54 ± 0.08
SSW	cut-on	$30.40 - 31.15$	31.30 ± 0.35
	cut-off	$52.08 - 53.19$	52.12 ± 0.37

the specifications within measurement uncertainty. Although the SSW low-wavenumber (long-wavelength) edges were found to be marginally outside of the specification, when combined with the high-wavenumber (short-wavelength) edges of the SLW waveband there remains an overlap of 2 cm^{-1} between the two detection bands, as required.

2.1.2 Instrumental Line Shape and Resolution

There are many definitions of resolution in the field of spectroscopy. One of the most widely used is the full width at half maximum (FWHM) of the instrumental line shape (ILS) of a spectrometer. This definition is well suited to spectrometers, such as a diffraction grating or a Fabry-Perot interferometer, whose ILS are not well defined. The Fourier transform spectrometer, however, possesses the best ILS of any spectrometer: the well-known *sinc* function. In Fourier transform spectroscopy, interferograms are recorded over a finite range of OPD determined by the length of the FTS translation stage, L. In this case FWHM of the ILS is given by[7]

$$\mathrm{FWHM} = \frac{1.207}{2L} \quad [\mathrm{cm}^{-1}], \tag{1}$$

demonstrating that the spectral resolution is inversely proportional to the maximum OPD.

The *sinc* function possesses secondary oscillations that decay in amplitude at increasing difference frequencies from the line centre. In fact, FTS spectral resolution may thus be enhanced if the information in the extended *sinc* ILS is used in the subsequent data analysis.

The ILS of an FTS is most easily probed by observing an unresolved spectral line source. In the PFM tests of the flight model (FM) SMEC, unresolved spectral line emission from both an infrared molecular laser and a photonic mixer were observed.[7] Figure 3 demonstrates a typical observation of a molecular laser line illustrating

the ideal *sinc* ILS of the SPIRE FTS. Due to time constraints and because the line source can only be focussed on one detector pixel at a time, measurements of the FWHM spectral resolution are only available for a limited set of the SLW and SSW pixels.

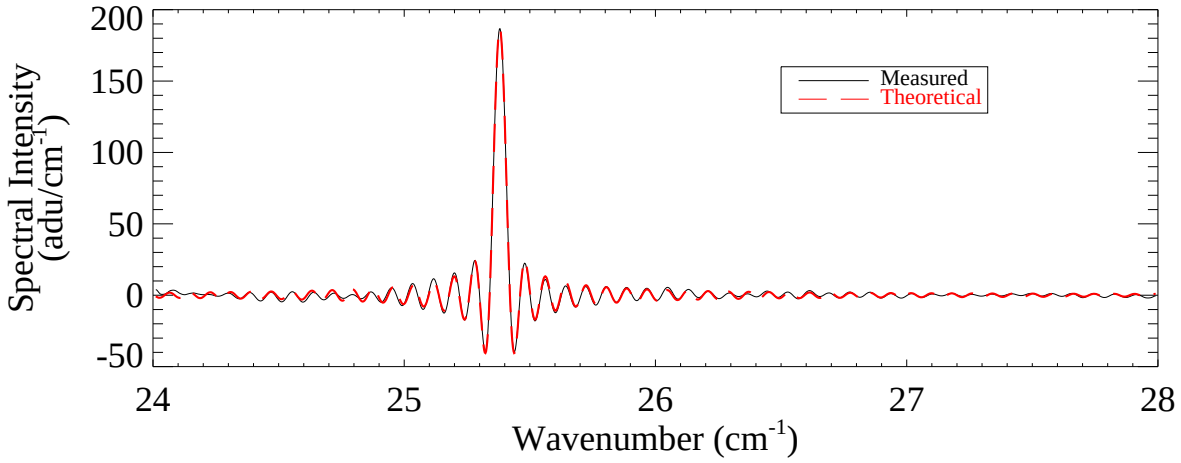

Figure 3. Measurements of an unresolved molecular laser line source (solid) and the theoretical *sinc* ILS (dashed).

Analysis of data similar to that of Figure 3 shows that the FM SMEC meets both the requirement and goal for maximum spectral resolution (0.04 cm^{-1} and 0.0483 cm^{-1} FWHM) within measurement uncertainty. Spectral resolution across the SPIRE arrays is shown in Figures 5 –5.

2.1.3 Minimum Resolution

While the original goal for the minimum spectral resolution was 4 cm^{-1}, it has since been realized that this results in such a low number of independent spectral data points that it will be difficult to correct for instrumental artefacts within the spectral passbands of the short and long wavelength arrays. For this reason, the minimum resolution of the SPIRE spectrometer during operations has now been set at 1 cm^{-1} which is readily achieved.[8]

2.1.4 Obliquity Effects

Divergence within an FTS gives rise to the Jacquinot criterion[9] where the product of the spectrometer resolving power, R, and divergent solid angle, Ω, are related by $R\Omega \leq 2\pi$. This phenomenon is known as natural apodization.

For the case of an on-axis pixel, natural apodization results in the interferogram being *multiplied* by a *sinc* function; or equivalently the spectrum being *convolved* with a rectangle function given by[10]

$$Rect(\sigma_r) = \int_{-\infty}^{+\infty} sinc\left(\frac{\sigma_o \Omega z}{2}\right) e^{-2\pi\sigma z} dz = \left(\frac{\pi}{\sigma_o \Omega}\right) Rect\left(\frac{\sigma_o \Omega}{2\pi}\right). \tag{2}$$

where σ_o is the frequency of the monochromatic source and Ω is the divergence within the interferometer. Thus, a monochromatic source of frequency σ_o will be observed to be centered at $\sigma_o[1 - \frac{\Omega}{4\pi}]$ with a width of $\frac{\sigma_o \Omega}{2\pi}$. An on-axis FTS detector with a field of view (FOV) of half-angle α will therefore observe an effective line centre σ_{obs} of

$$\sigma_{\mathrm{obs}} = \sigma_o \left(1 - \frac{\alpha^2}{4}\right) \quad [\mathrm{cm}^{-1}] \tag{3}$$

for a monochromatic source of frequency σ_o.[11]

In the case of an off-axis pixel, the effective OPD is less than that for the axial ray by a factor of $\cos\beta$ (where β is the angle of the ray from the optical axis of the interferometer with respect to the pupil) and the computation of the FTS natural apodization becomes more complex.[12] However, to first order, the ILS computation may be simplified. For oblique rays transiting the interferometer, the frequency of a monochromatic source on a non-central detector, ignoring the line shift due to the FOV, will occur at

$$\sigma_{\rm obs} = \sigma_o \cos(\beta) \quad [\mathrm{cm}^{-1}]. \tag{4}$$

To a first approximation, the combined effects of a finite detector FOV (α) and off-axis angle (β) on the observed line centre may be expressed as[13]

$$\sigma_{\rm obs} = \sigma_o \left[1 - \left(\frac{\beta^2}{2} + \frac{\alpha^2}{4}\right)\right] \quad [\mathrm{cm}^{-1}]. \tag{5}$$

Figure 4 shows the normalized axial variation of various molecular laser line centres plotted against the detector angular position on the sky. This figure also shows the expected shift as a function of off-axis angle for both the SLW and SSW arrays.

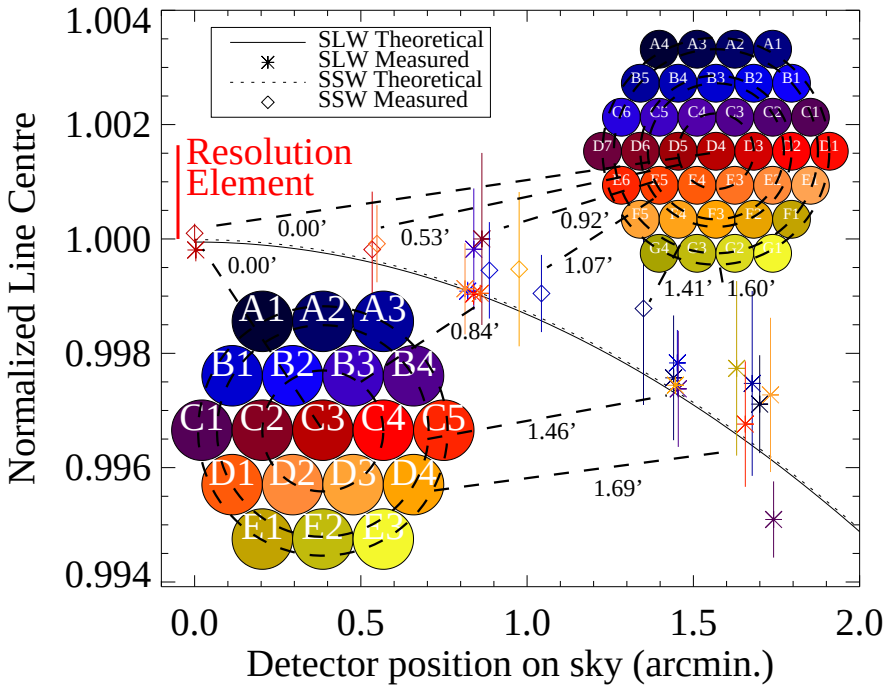

Figure 4. Normalized theoretical and measured line centre shift as a function of SPIRE detector angular position. Also shown are the two detector arrays with dashed rings indicating the detectors of equivalent axial orientation, with their central off-axis sky position shown on the line tracing the ring to its location on the line centre curve, SLW has 3 concentric rings while SSW has 5.

Another goal for the SPIRE off-axis detectors is that their measured resolution not exceed 110% of the maximum axial FWHM resolution (i.e. 0.0531 cm^{-1} cf. 0.0483 cm^{-1}). Although some pixels lie outside of the unvignetted field of view, for those pixels where a monochromatic source was observed, this goal has been achieved within measurement uncertainty as shown in Figure 5.

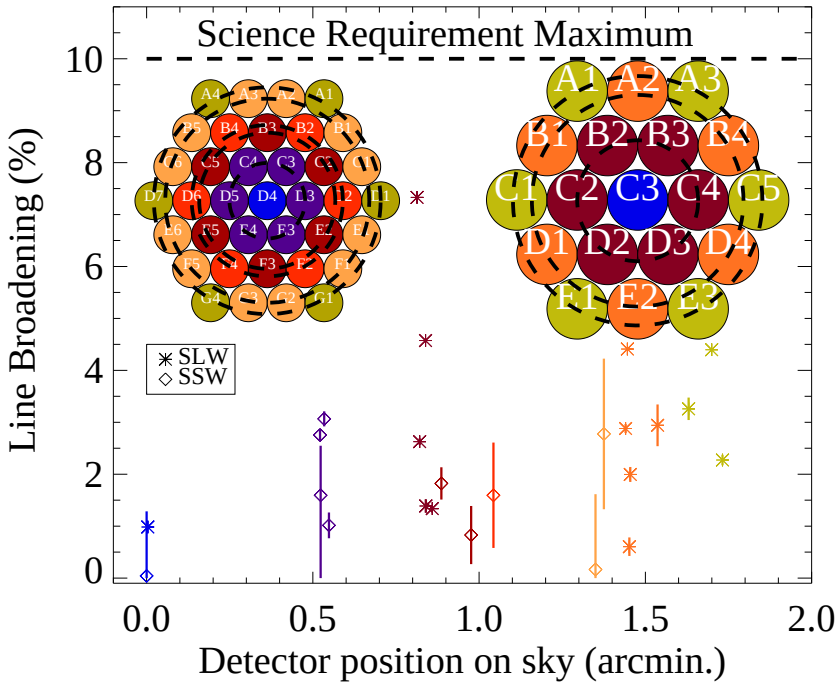

Figure 5. Line broadening across the SPIRE arrays. The detectors within the unvignetted FOV observe FWHM line broadening within specification.

2.1.5 Vignetting

Vignetting, defined as the loss of power for off-axis pixels at high optical path differences, was observed in data from each of the PFM test campaigns. At the required resolution of 0.4 cm^{-1}, the baseline of the measured interferograms was found to be uniform to within 2%, meeting the requirement of <10% uniformity (see Table 2). At the maximum spectral resolution for the SPIRE spectrometer, uniformity to within 10% was measured on all of the pixels that lie within the unvignetted field of view as well as on most of the pixels that lie outside of this field of view. Figure 6 illustrates the measured vignetting for all active channels from the PFM4 test campaign.

2.1.6 In-band Stray Light

Throughout the PFM test campaign phase, the major cause of in-band spectral straylight has been attributed to the presence of channel fringes.[6,7] The channel fringes can be traced to a resonant cavity formed by the entrance apertures of the feedhorn arrays and the surface(s) of the field lens which is used to render the beam telecentric.[14] In order to quantify this straylight contamination, the integrated spectral power was derived from those portions of the measured interferograms that contain channel fringes. This fringe spectral power was then compared to the integrated spectral power derived from the portion of the interferogram near the position of zero path difference (ZPD), which was considered to be free of channel fringes. Further study of the PFM4 data has shown that for all active pixels, with the exception of pixel SLWC3, the ratio of the in-band channel fringe spectral power to that of the source is less than 4%, meeting the <5% requirement.[5] In the case of only one pixel, SLWC3, the central pixel of the SLW array, the ratio was found to be 6%, slightly exceeding the <5% straylight requirement.

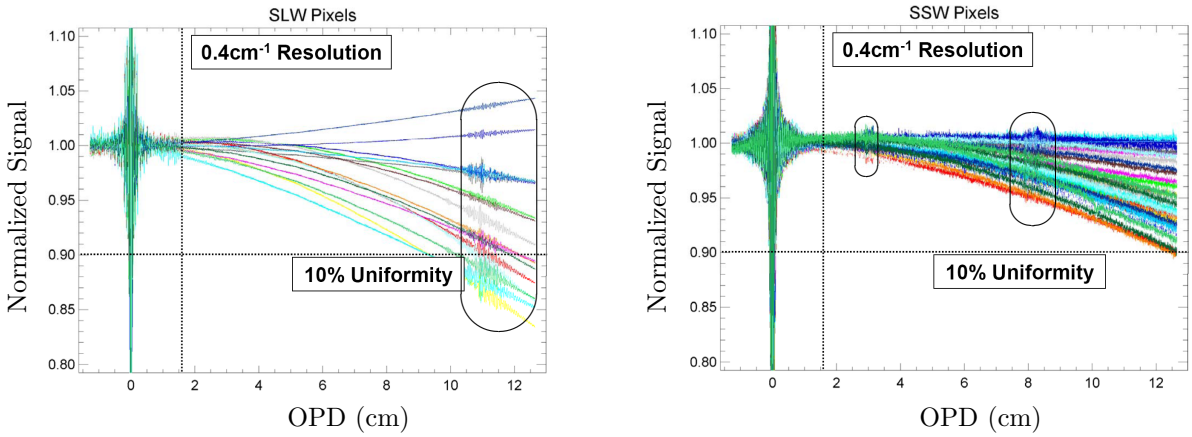

Figure 6. SLW (left) and SSW (right) interferograms demonstrating illumination vignetting across the detector arrays. The circled regions represent channel fringes that are discussed in section 2.1.6.

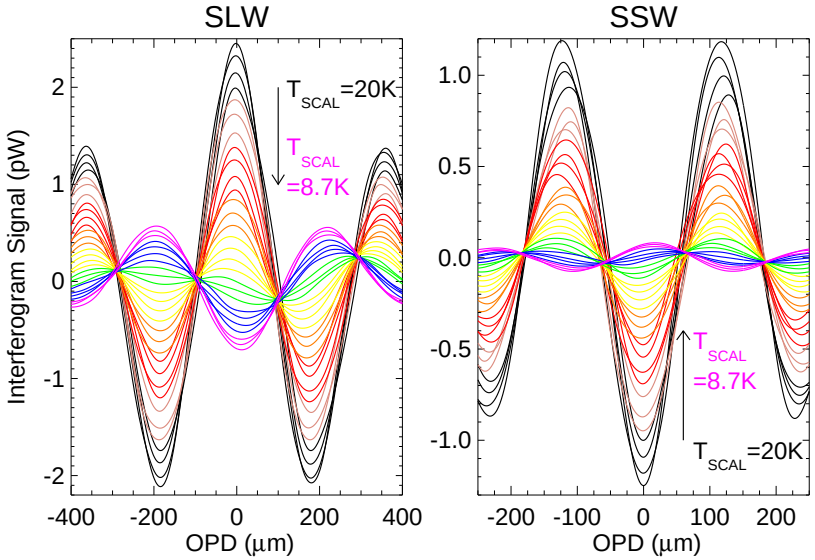

Figure 7. Series of interferograms for both SLW (left) and SSW (right) with the CBB held at 6.7 K while SCAL cools from an initial temperature of 20 K.

2.2 Input Port Balancing

For broad-band/continuum observations, the challenging dynamic range requirements of the interferogram signal near ZPD can be reduced by port balancing, a technique in which a broadband spectral source is placed at the second, complementary FTS input port. SPIRE's imaging FTS uses a calibration source (SCAL) at its second input port in order to compensate for the blackbody emission of the passively cooled Herschel telescope observed through the primary input port.[15] Port balancing is particularly advantageous in cases where blackbody emission from the input optics of an interferometer produce a radiative background which dominates a much weaker source signal, a case frequently found in far-infrared and submillimetre astronomy.

In order to demonstrate port compensation with the SPIRE FTS, a series of interferograms were recorded with the CBB held constant at a temperature of 6.7 K while SCAL was allowed to cool from an initial temperature of 20 K. The results are shown in Figure 7 from which two important aspects of the Mach-Zehnder[1] design are seen clearly. The first is the complementary nature of the signal at the two output ports. The second is the effective nulling of the modulated component of the signal as SCAL cools to approach the temperature of the

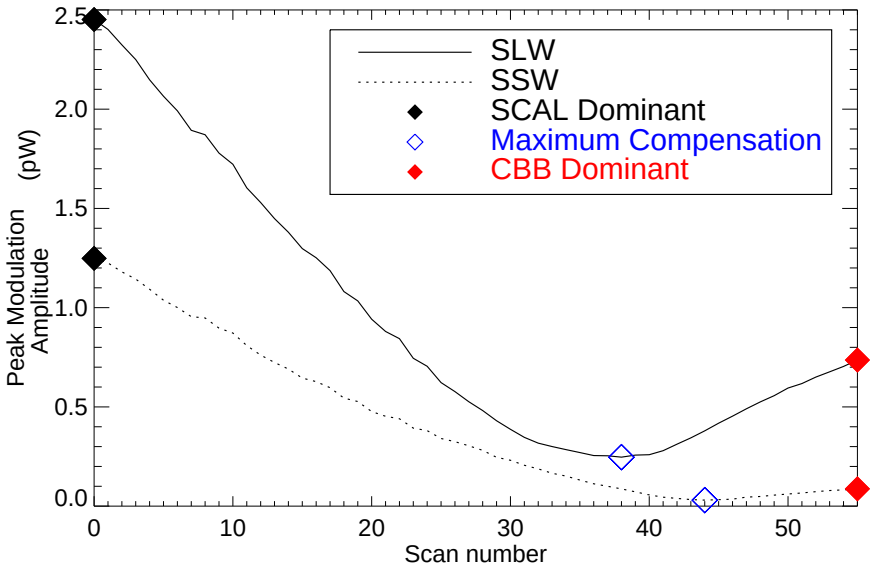

Figure 8. Interferogram peak modulation amplitude for the series of interferograms shown in Figure 7.

CBB. The peak modulation amplitude of each scan as SCAL is cooling is shown in Figure 8; here the local minima demonstrates optimal input port balancing/compensation.

The PFM tests have shown that, while the SCAL sub-system is capable of compensating for the emission from the laboratory CBB source, the compensation occurs at different temperatures for pixels in the same detector array.[6] In addition, the range of temperatures over which spectral compensation was achieved was different for the two detector arrays (see Figure 8). As a result, it will be necessary to choose a temperature that, while not optimal for any given pixel, is optimal for the two detector arrays as a whole taking into account the complex issues of calibration and phase correction for the measured interferograms.

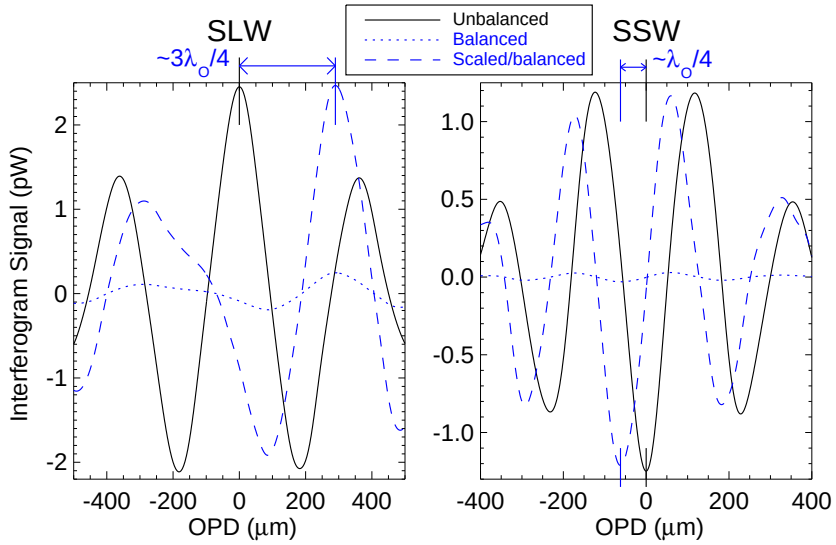

Figure 9. Input dominant (solid) and beamsplitter emission dominant (dotted) interferograms observed in PFM testing with the SPIRE FTS. The beasmplitter emission dominant case has been scaled (dashed) to the input dominant amplitude to better enable comparison.

It has been shown that, when the input ports are well balanced, emission from the first beamsplitter can make a significant contribution to the overall measured interference signal.[16] Furthermore, this signal is out of phase with the input port contributions of the interferogram by ~$\pi/2$ (see Figure 9) and must be removed in data processing prior to final Fourier transformation.[15]

It should be noted that compensation studies to date have by necessity involved the CBB and not the actual telescope. As such, the final SCAL settings for the optimal spectral compensation will only be identified in flight once the temperature and emissivity of the Herschel telescope have been determined.

2.2.1 Fringe Contrast

During the PFM4 test campaign, a laboratory infrared laser was used to study the interferometer modulation efficiency as a function of OPD, i.e. fringe contrast. As was the case for the infrared laser during the PFM1 and PFM3 test campaigns, only a subset of the pixels in each spectrometer detector array was directly illuminated with the laser. Figure 10 illustrates an observed interferogram where the molecular laser[7] was used to illuminate one of the SPIRE detectors. The results of these tests, illustrated in Figure 11, show that for pixels within the unvignetted field of view the measured fringe contrast exceeds the specification of >80%[3] and the predicted value of 87%.[17]

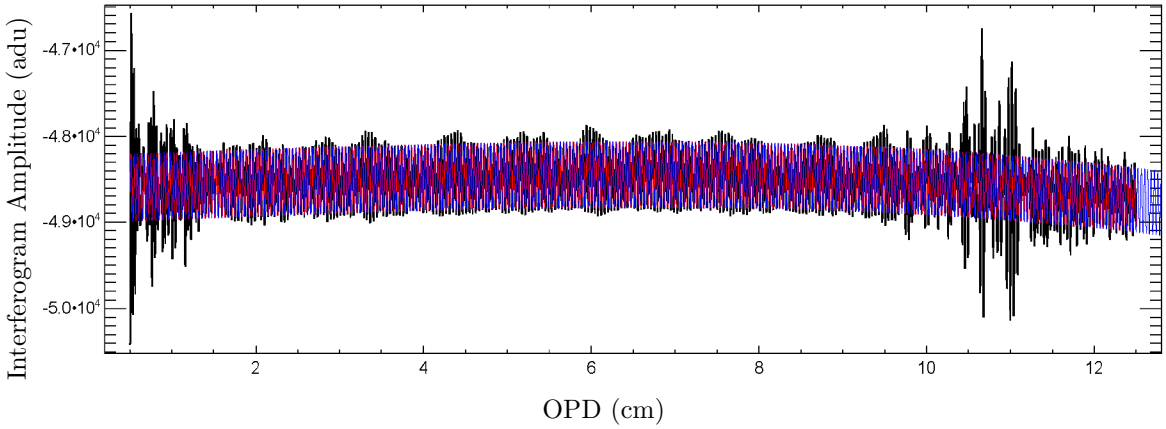

Figure 10. A SPIRE interferogram with sinusoidal fit representative of those used to determine fringe contrast.

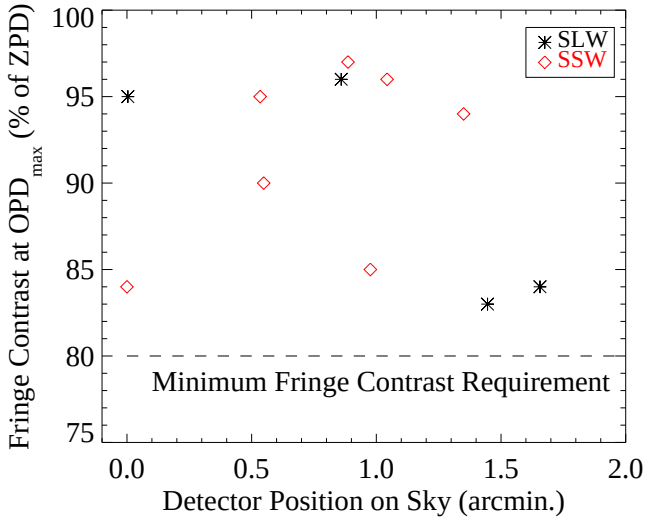

Figure 11. Observed Fringe contrast across the SPIRE arrays.

2.2.2 Optical Performance Summary

The SPIRE spectrometer has been verified to be compliant with its science-driven performance requirements. The spectrometer performance requirements are summarized in Table 2, with ✓'s indicating those requirements that have been met.

Table 2. SPIRE performance specifications

Reference number[3]	Description	Requirement	Status
IRD-SPEC-R01	Wavelength	SSW:$200 - 300$ μm, $33.3 - 50.0$ cm^{-1}	Marginal
	Range	SLW:$300 - 670$ μm, $14.9 - 33.3$ cm^{-1}	✓
IRD-SPEC-R02	Maximum Resolution	Req.: 0.4 cm^{-1}	✓
		Goal: 0.0483 cm^{-1}	✓
IRD-SPEC-R03	Minimum Resolution	Req.: 2 cm^{-1}	✓
		Goal: 1 cm^{-1}	✓
IRD-OPTS-R07	Balancing of Output Ports	Beamsplitters shall have $2RT = R^2 + T^2$ to within 90% over the band	✓
IRD-OPTS-R09	Straylight	$< 5\%$ of total in-band power	✓
IRD-SPEC-R10	Off-Axis Resolution	FWHM $< 110\%$ of nominal resolution	✓
IRD-SPEC-R11	Vignetting	$< 10\%$ uniformity for $R = 0.4$ cm^{-1}	✓
IRD-SPEC-R14	Fringe Contrast	$> 80\%$ for $R = 0.4$ cm^{-1}	✓

Although great efforts have been employed to ensure that SPIRE will perform successfully in a space environment, the in-orbit performance awaits the performance verification (PV) phase of the mission which starts shortly after launch. Performance specifications to be determined after launch include: temperature, emissivity, and straylight of the Herschel primary mirror; the SCAL compensation scheme; the SPIRE spectrometer vibration/noise environment during flight; and the performance of critical subsystems. Thus, many instrument performance characteristics and calibration data products will only be known precisely after launch.

2.3 SPIRE Mechanism

The performance of the SPIRE mechanism has been evaluated through specific subsystem level test and through operation of the SPIRE spectrometer. Individual characteristics such as sample interval, sampling step control, scan length, and mirror velocity control and stability were shown to perform satisfactorily for all of its requirements (Table 3, ✓'s indicate those requirements that have been met). Although it has been shown that SMEC will operate adequately under step–and–integrate scanning mode,[5] this is currently being considered as a back-up operational mode and will not be implemented during standard operations. Optimization of the proportional–integral–derivative (PID) servo control of the SMEC will be performed during the PV phase after launch.

3. CONCLUSIONS

Results from the PFM test campaigns related to the SPIRE imaging FTS have been presented. The passband regions for both arrays fall mostly within specification; regions outside of specification fall very near to it. There is sufficient SLW/SSW spectral overlap for cross-calibration of all co-aligned detectors. Spectrometer spectral resolution across both arrays is within specification and follows behaviour predicted by theory, as is shown by analysis of the ILS, both on and off the optical axis. The SPIRE spectrometer exceeds vignetting requirements by at least an order of magnitude in all cases; fringe contrast requirements have also been met. The SPIRE SMEC has also been demonstrated to perform within specifications.

Table 3. SPIRE SMEC performance specifications

Reference number[3]	Description	Requirement	Status
IRD-SMEC-R01	Linear Travel	14 cm OPD	✓
IRD-SMEC-R02	Min. Sampling Interval (μm)	SSW: 5 SLW: 7.5	✓
IRD-SMEC-R03	Sampling Step Control (μm)	Variable between 5 and 25	Non-standard AOT
IRD-SMEC-R04	Scan Length	Able to scan from either side of ZPD	✓
IRD-SMEC-R05	Dead-time	$< 10\%$ for 0.4 cm^{-1} resolution	N/A
IRD-SMEC-R06	Mirror Velocity	Req. 0.1 cm/s MPD goal 0.2 cm/s MPD	✓ TBD
IRD-SMEC-R07	Velocity Control	Selectable from 0 to 0.1 cm/s MPD	✓
IRD-SMEC-R08	Velocity Stability	$< 10\mu$m/s over the full range	✓
IRD-SMEC-R09	Position Measurement	0.1 μm within $\pm$0.32 cm OPD, 0.3 μm elsewhere.	✓ ✓

During the PFM test campaigns, two areas have been identified that will require further study to optimize the scientific return from the SPIRE FTS: channel fringe removal and beamsplitter emission. Algorithms are currently being developed for the removal of channel fringes and their deleterious effects on the resulting spectra.[18] A study of the effects of beamsplitter emission is currently underway in our laboratory using a Mach-Zehnder FTS of similar design to that of SPIRE. The goal of this study is to develop a schema for removal of the contribution of beamsplitter self-emission to the signal that will be measured with SPIRE.

Following the much anticipated launch of Herschel, the observatory will enter a PV phase. During this phase of the mission, SPIRE will conduct basic functional and calibration tests to replicate those conducted on the ground, and for the first time operate under the environmental conditions for which the instrument was designed. The SPIRE instrument will conduct a series of FTS scans with various SCAL settings observing the primary mirror as it cools in order to understand and calibrate for the blackbody emission of the Herschel optics. These tests will also provide important information for the removal of channel fringes and beamsplitter emission from the observed interferograms. SPIRE will also perform high-resolution scans of several astronomical calibration sources.

At the time of writing this paper, flight model testing of all Herschel science instruments is completed, the Herschel telescope is fully assembled, and Herschel integration testing is being performed by ESA; performance evaluation testing of the SPIRE flight spare model has also commenced.

4. ACKNOWLEDGEMENTS

The authors wish to thank Steve Guest for his valuable assistance with the database and Java; Asier Aramburu and Sunil Sidher for their assistance with the SPIRE database, as well as all of the long hours in the control room; Matt Griffin *et al.* in Cardiff for useful feedback during the SDAG meetings and otherwise; Ken King and Dave Smith for their managerial assistance; Sarah Leeks and Ivan Valtchanov for their dedication to instrument testing; Alan Pearce and Mike Trower for their technical assistance; as well as the countless others who form the SPIRE group within the SSTD at RAL, and the SPIRE consortium in general. This research has been funded by CSA, NSERC, AI, STFC, CIPI, and CFI.

REFERENCES

[1] Griffin, M., Swinyard, B., and Vigroux, L., "The SPIRE Instrument for FIRST," in [*UV, Optical and IR Space Telescopes and Instruments, Proc. SPIE*], Breckinridge, J. B. and Jakobsen, P., eds., **4013**, 184–195, International Society for Optical Engineering (Mar 2000). SPIE symposium, 29-31 March 2000.

[2] Pilbratt, G. L., "Herschel Mission Overview and Key Programmes," in [*Space Telescopes and Instrumentation I: Optical, Infrared, and Millimeter Wave 2008*], **7010**, Proceedings of the International Society for Optical Engineering (2008).

[3] Swinyard, B. M. and King, K., "SPIRE Instrument Requirements Document," tech. rep., Rutherford Appleton Laboratory, Chilton, Didcot, Oxfordshire, UK (July 2005). SPIRE-RAL-PRJ-000034.

[4] Lim, T. L., Swinyard, B. M., Griffin, M., Aramburu, A. A., Baluteau, J.-P., Bock, J. J., Ferlet, M. J., Fulton, T. R., Griffin, D., Guest, S., Hargrave, P., King, K., Leeks, S., Naylor, D. A., Polehampton, E. T., Rizzo, D., Sawyer, E., Schulz, B., Sidher, S., Spencer, L. D., Smith, D., Nguen, H. T., Valtchanov, I., Waskett, T., and Woodcraft, A., "Preliminary results from Herschel-SPIRE flight model testing," in [*Space Telescopes and Instrumentation I: Optical, Infrared, and Millimeter*], **6265**, Proceedings of the International Society for Optical Engineering (2006).

[5] Baluteau, J.-P., Fulton, T. R., and Naylor, D. A., "SPIRE Science Verification Review: SMEC and Spectrometer Performance," tech. rep., Laboratoire d'Astrophysique de Marseille, Blue Sky Spectroscopy, University of Lethbridge (October 2007).

[6] Naylor, D. A., Baluteau, J.-P., Davis-Imhof, P., Ferlet, M. J., Fulton, T. R., and Swinyard, B. M., "Performance evaluation of the Herschel/SPIRE imaging Fourier transform spectrometer," in [*Space Telescopes and Instrumentation I: Optical, Infrared, and Millimeter*], **6265**, Proceedings of the International Society for Optical Engineering (2006).

[7] Spencer, L. D., Naylor, D. A., and Swinyard, B. M., "A comparison of the theoretical and measured performance of the Herschel/SPIRE imaging Fourier transform spectrometer," in [*Space Telescopes and Instrumentation I: Optical, Infrared, and Millimeter*], **6265**, Proceedings of the International Society for Optical Engineering (2006).

[8] Naylor, D. A., "Spectrometer Performance Review," tech. rep., University OF Lethbridge, Lethbridge, Alberta, Canada (July 2005). Presentation for the SPIRE Consortium Meeting, Caltech.

[9] Jacquinot, P., "New developements in interference spectroscopy," *Rep. Prog. Phys.* **23**, 267–312 (1960).

[10] Bell, R. J., [*Introductory Fourier Transform Spectroscopy*], Academic Press, New York (1972).

[11] Davis, S. P., Abrams, M. C., and Brault, J. W., [*Fourier Transform Spectroscopy*], Academic Press, first ed. (2001).

[12] Genest, J. and Tremblay, P., "Instrument Line Shape of Fourier Transform Spectrometers: Analytic Solutions for Nonuniformly Illuminated Off-Axis Detectors," *Appl. Opt.* **38**(25), 5438–5446 (1999).

[13] Fulton, T. R., "Obliquity in the SPIRE Spectrometer," tech. rep., Blue Sky Spectroscopy, Lethbridge, Alberta, Canada (March 2008).

[14] Swinyard, B., Dohlen, K., Ferand, D., Baluteau, J. P., Pouliquen, D., Dargent, P., Michel, G., Martignac, J., Ade, P., Hargrave, P., Griffin, M., Jennings, D., and Caldwell, M., "The Imaging FTS for Herscel SPIRE," in [*IR Space Telescopes and Instruments, Proc. SPIE*], **4850**, 698–709 (Mar 2003).

[15] L.D. Spencer *et al.*, "Port compensation using the Herschel/SPIRE imaging Fourier transform spectrometer," IRMMW-THz, IEEE, Cardiff, UK (2007).

[16] Carli, B., Palchetti, L., and Raspollini, P., "Effect of beam-splitter emission in Fourier-transform emission spectroscopy," *Applied Optics* **38**, 7475–7480 (Dec. 1999).

[17] Griffin, D., Griffin, M., and Swinyard, B., "SPIRE Design Description," Tech. Rep. SPIRE-RAL-PRJ-000620, Rutherford Appleton Laboratory (May 2003).

[18] Fulton, T. R., Naylor, D. A., Baluteau, J.-P., Griffin, M., Davis-Imhof, P., Swinyard, B., Lim, T. L., Ordenovic, C., Surace, C., Clements, D., Panuzzo, P., Gastaud, R., Polehampton, E. T., and Guest, S., "The data-processing pipeline for the Herschel/SPIRE Fourier Transform Spectrometer," in [*Space Telescopes and Instrumentation I: Optical, Infrared, and Millimeter Wave 2008*], **7010**, Proceedings of the International Society for Optical Engineering (2008).